Correlation of helicopter rotor aeroelastic response with HART-II wind tunnel test data

A. Arun Kumar S.R.Viswamurthy and Ranjan Ganguli *

Department of Aerospace Engineering, Indian Institute of Science, Bangalore-560012, India

Abstract

This paper compares predictions of a comprehensive aeroelastic analysis for a helicopter rotor with Higher Harmonic Control Aeroacoustic Rotor Test (HART-II) data. The HART-II test was performed in Large Low speed Facility (LLF) of the German-Dutch Wind Tunnel (DNW) as a part of an international co-operative program. The HART-II data was made available in the public domain for code validation and improvement studies by researchers. The comprehensive aeroelastic analysis used here is based on finite element method in space and time. Moderate deflection and Coriolis non-linearities are included in the analysis. For aerodynamic modeling, free wake and unsteady aerodynamic models are used. Numerical results for blade natural frequencies and mode shapes are first compared with the results obtained through HART-II tests. The blade flap, lead-lag and torsion response are compared at low speed flight condition with both HART-II test data and other aeroelastic analyses.

1 Introduction

Engineering analysis has become a very important tool in design in recent years. Typically, such analyses are developed as software which predict the real system behaviour. However, before such a software can be widely used for design, there is a need to validate it with experimental data. Validation is the process of determining the degree to which a model or simulation is an accurate representation of the real world from the perspective of intended uses of the model or simulation. Validation leads to an estimate of the gap between the result of the simulation and the actual physical behaviour. A knowledge of this gap can lead to an estimate of the margins of error in the design process.

The accurate prediction of the helicopter rotor blade dynamic and aeroelastic behaviour is an important practical problem which is very challenging due to the coupling between the highly flexible rotating blade and an unsteady aerodynamic environment. Most helicopter companies, several aerospace research labs and a few universities have developed comprehensive aeroelastic analysis to model the helicopter. For example, the analyses such as Second Generation Comprehensive Helicopter Analysis System (2GCHAS) [1,2] and Comprehensive Analytical Model of Rotorcraft Aerodynamics And Dynamics (CAMRAD-II) [3,4] are widely used for helicopter aeroelastic response. In particular, Lim et. al. [4] compared CAMRAD-II pre-

* Associate Professor; Corresponding author; Email: ganguli@aero.iisc.ernet.in; Address: Department of Aerospace Engineering, Indian Institute of Science, Bangalore-560012, India; Phone: +918022933017; Fax: +918023600134.

dictions with HART-I wind tunnel test data with single and multiple trailer wake models. The HART rotor was a 40 percent, Mach scaled model of the hingeless BO105 rotor. The multiple trailer wake model was found to give better prediction of the lift distribution. A recent international effort in validation involved the Westland Lynx helicopter rotor [5]. In this work, frequencies and vibratory hub load prediction from different codes were compared with the flight test results. The use of free wake modeling was found to be necessary in improving the analysis prediction.

In general, the geometry and properties of a real rotor blade are quite complex. In such cases, it is difficult to isolate the cause of the prediction problems. Therefore, some researchers have looked at comparing analysis predictions with wind tunnel tests which use blades with simple geometry. Ganguli et. al. [6] used the Vibration Attenuation through Structural Tailoring (VAST) data [7,8] to validate the University of Maryland Advanced Rotorcraft Code (UMARC) aeroelastic analysis. The VAST data used model rotors with different mass and stiffness properties and vibratory loads were measured for the different rotors. The aim was to experimentally validate a blade design obtained using modal based optimization. They found that while the analysis underpredicted vibration, it was able to account for the influence of mass and stiffness changes of the blade on the vibrating loads. Again, free wake model was found to be important for vibration predictions. Datta and Chopra [9] used the UH-60A flight test data to validate structural and aerodynamic modeling. The lower harmonic torsion moments and pitch link loads were well predicted, though deficiencies existed for torsion loads above 4/rev. The predictions were sensitive to the wake model and trim state.

In recent years, Higher Harmonic Control (HHC) has been proved to be effective in reducing helicopter noise and vibration [10,11]. The HART-II tests provide blade response data for a baseline rotor with primary control as well as for different HHC forcing. In this study, the experimental data for the 4 bladed HART-II rotor is used to validate a version of the UMARC comprehensive aeroelastic analysis. A systematic study and validation of the blade rotating frequencies is first done and then mode shapes are predicted by the finite element model for the non-uniform rotor blade. Next, the nonlinear response predictions are compared with the test data and with predictions from other analyses such as CAMRAD-II, HOST and S4.

2 Experimental Data

The HART-II results have been extensively documented in the literature [12–18]. Also, the HART-II data is available for use by the research community from the DLR. The HART-II test was conducted in the open-jet configuration of 8m by 6m cross section in the large anechoic testing hall. The maximum achievable airspeed for HART-II was 85m/s, but the air speed during the actual HART-II test was 33m/s. The HART-II test used a 40 percent Mach scaled, four bladed hingeless BO105 model rotor. It was aeroelastically scaled such that the model rotor blade matched the natural frequencies of the full scale model for the first three flap, first two lead-lag and first torsion modes. The blades are rectangular with -8 degree of built in linear twist and a precone of 2.5 degree as in the full scale rotor. The nominal operating speed was 1041 rpm and the hover tip Mach number was 0.641. A brief description of the HART-II rotor properties is given in Table 1 and cross sectional properties at different stations are given in Table 2. Fig. 1 shows the sign convention for centre of gravity, tension centre and aerodynamic center offsets and the offset values at different radial stations are given in Table 3. It can be observed that the blade root section shows considerable variation in elastic properties and the properties of outboard section of the blade are quite uniform.

Table 1
Rotor Properties

Rotor Radius, R	2 m
Number of blades, N_b	4
Blade Chord, c	0.121 m
Solidity, σ	0.077
Root cutout	0.44 m
C_T/σ	0.0571
Blade Airfoil	modified NACA23012

Table 2
Rotor stiffness and inertia properties at different radial stations along the blade.

Station	EI_y	EI_z	GJ	Mass per unit length	Radius of gyration	
m	N-m^2	N-m^2	N-m^2	Kg/m	Edgewise(m)	Flapwise(m)
0.00	3000	14000	380	3.67	0.00738	0.00738
0.075	3000	14000	380	3.67	0.00738	0.00738
0.15	675	3390	380	1.57	0.01378	0.00098
0.19	675	4420	442	1.57	0.01378	0.00098
0.24	675	5370	500	1.72	0.01530	0.00109
0.29	594	5930	460	1.71	0.01588	0.00113
0.34	480	6610	390	1.67	0.01607	0.00115
0.39	400	5710	320	1.47	0.01822	0.00130
0.415	290	5710	280	1.45	0.02071	0.00148
0.44	250	5200	160	0.95	0.02617	0.00187
2.00	250	5200	160	0.95	0.02617	0.00187

Table 3
Offset values at different radial stations along the blade.

Station	e_g	e_A	e_d
m	m	m	m
0.00	0.00000	0.00000	0.00000
0.075	0.00000	0.00000	0.00000
0.15	0.00000	0.00000	0.00000
0.19	0.00000	0.00000	0.00000
0.24	0.00060	0.00330	0.00000
0.29	0.00180	0.00370	0.00195
0.34	0.00190	0.00430	0.00415
0.39	0.00440	0.00730	0.00625
0.415	0.00290	0.00920	0.00835
0.44	-0.00550	0.00030	- 0.00535
2.00	-0.00550	0.00030	- 0.00535

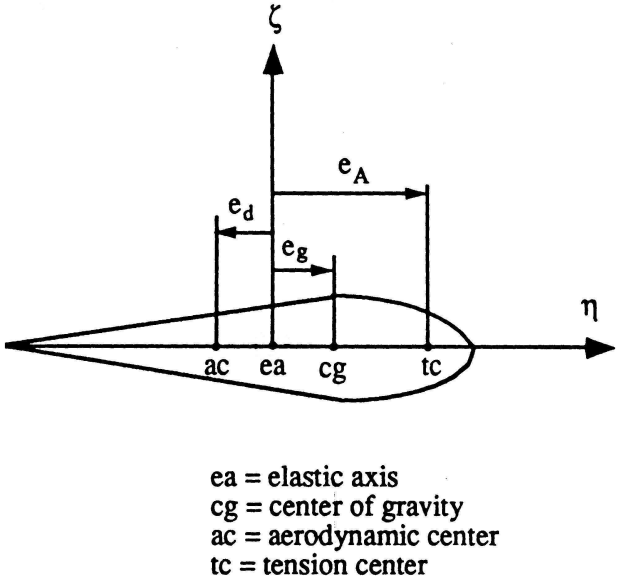

Fig. 1. Sign convention for c.g, t.c and a.c offsets

In HART-II, a new technique called Stereo Pattern Recognition(SPR) for non-intrusive optical measurement was applied to measure blade deflections in flap, lead-lag and torsion modes. This new technique is based on the recognition and tracking of visible markers on the blade surface using stereometric camera systems. The camera systems are calibrated by setting up a matrix of calibration markers with known positions in 3-dimensional space.

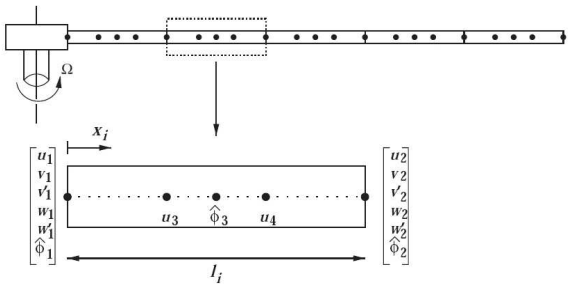

Fig. 2. The 15-DOF finite element model used for spatial discretization of the beam

By means of 4 cameras which were triggered to the rotor azimuth, and a sequence of 18 markers distributed along the leading edge of the rotor blades, their position co-ordinates in space can be evaluated from the camera images. As a result, the flap and lead-lag deflection of the blade can be computed directly. Furthermore, the elastic torsion of the blade can be extracted by subtracting the commanded pitch at the blade root and the built-in pre-twist.

3 Comprehensive Aeroelastic Analysis Code

University of Maryland Advanced Rotorcraft Code (UMARC) is a comprehensive code for the aeroelastic analysis of a helicopter rotor and is based on the finite element methodology. The helicopter is modeled as several elastic blades attached to a rigid fuselage. The blade undergo flap bending, lag bending, elastic twist and axial deformation. For analysis, the blade is discretized into N beam elements and each element consists of 15 degrees of freedom as shown in Figure 2. Also, the formulation accounts for chordwise offsets of blade section center mass, tension center and aerodynamic center from the elastic axis.

The finite element formulation is based on Hamilton's principle, which can be written as

$$\int_{\psi_1}^{\psi_2} (\delta U - \delta T - \delta W) d\psi = 0 \qquad (1)$$

where δU, δT and δW are the virtual strain energy, virtual kinetic energy and virtual

work of the system respectively. The δU, δT include energy contributions from components that are attached to the blade, e.g.,pitch link, lag damper etc, and are shown in the Appendix. External aerodynamic forces on the rotor blade contribute to the virtual work variational, δW. For the aeroelastic analysis, detailed unsteady aerodynamics and free wake models are used. The effect of compressibility and reversed flow are also included in the aerodynamic model.

Discretization of Hamilton's principle in Eq.(1) yields,

$$\int_{\psi_1}^{\psi_2} \sum_{i=1}^{N} (\delta U_i - \delta T_i - \delta W_i) d\psi = 0 \qquad (2)$$

where δU_i, δT_i and δW_i are the elemental virtual energy contribution and N is the number of beam spatial finite elements. The fifteen degrees of freedom are distributed over five element nodes (two boundary and three interior nodes). There are six degrees of freedom at each element boundary node, these six degrees of freedom corresponds to $u, v, v', w, w', \hat{\phi}$. There are two internal nodes for axial deflection u, and one internal node for elastic twist $\hat{\phi}$. These degrees of freedom correspond to cubic variations in axial elastic and bending (flap and lag) deflections, and a quadratic variation in elastic twist. Between the elements there is continuity of slope and displacement for the flap and lag bending deflections and continuity of displacements for the elastic twist and axial deflections. This element ensures physically consistent linear variations of bending moments and torsion moments and quadratic variations of axial force within each element. Using the interpolating polynomials, the distribution of deflections over a beam element is expressed in terms of the elemental nodal displacements q_i. For the ith beam element, the shape functions are given by,

$$\mathbf{u}(s) = \begin{Bmatrix} u(s) \\ v(s) \\ w(s) \\ \hat{\phi}(s) \end{Bmatrix} = \begin{bmatrix} \mathbf{H_u} & 0 & 0 & 0 \\ 0 & \mathbf{H} & 0 & 0 \\ 0 & 0 & \mathbf{H} & 0 \\ 0 & 0 & 0 & \mathbf{H}_{\hat{\phi}} \end{bmatrix} \mathbf{q_i} \qquad (3)$$

where the elemental nodal displacement vector is defined as

$$\mathbf{q_i}^T = \begin{bmatrix} u_1 & u_2 & u_3 & u_4 & v_1 & v_1{}' \end{bmatrix}$$

$$\mathrm{v}_2 \quad v_2{}' \quad w_1 \quad w_1{}' \quad w_2 \quad w_2{}' \quad \hat{\phi}_1 \quad \hat{\phi}_2 \quad \hat{\phi}_3 \qquad (4)$$

The interpolating polynomials for shape functions in Eq.(3) are given as

$$\begin{aligned} \mathbf{H_u} &= (-4.5s^3 + 9s^2 - 5.5s + 1, 13.5s^3 \\ &- 22.5s^2 + 9s - 13.5s^3 + 18s^2 \\ &- 4.5s, 4.5s^3 - 4.5s^2 + s) \\ \mathbf{H} &= (2s^3 - 3s^2 + 1, l_i(s^3 - 2s^2 + s), \\ &- 2s^3 + 3s^2, l_i(s^3 - s^2)) \\ \mathbf{H}_{\hat{\phi}} &= (2s^2 - 3s + 1, -4s^2 + 4s, 2s^2 \\ &- s) \end{aligned} \qquad (5)$$

where $s = x_i/l_i$ and l_i is the length of the ith beam element.

Assembling the blade finite element equations and applying boundary conditions results in Eq. (2) becoming

$$\mathbf{M}\ddot{\mathbf{q}}(\psi) + \mathbf{C}(\psi)\dot{\mathbf{q}}(\psi) + \mathbf{K}(\psi)\mathbf{q}(\psi) = \mathbf{F}(\mathbf{q}, \dot{\mathbf{q}}, \psi) \qquad (6)$$

The above equation represents a parametric nonlinear differential equation. The damping and stiffness matrices become time dependent due to aerodynamic motion dependent forces, the linear parts of which have been moved to the left hand side. The nodal displacements $\mathbf{q}$ are functions of time and all non-linear terms have been moved into the

force vector in the right-hand side. The spatial functionality has been removed by using finite element discretization and partial differential equations have been converted to ordinary differential equations. The finite element equations representing each rotor blade are transformed to normal mode space for efficient solution of blade response using the modal expansion. Typically, 6-10 modes are used. The displacements are expressed in terms of normal modes as

$$\mathbf{q} = \mathbf{\Phi p} \tag{7}$$

Substituting Eq. (9) into Eq. (8) leads to normal mode equations having the form

$$\bar{\mathbf{M}}\ddot{\mathbf{p}}(\psi)+\bar{\mathbf{C}}(\psi)\dot{\mathbf{p}}(\psi)+\bar{\mathbf{K}}(\psi)\mathbf{p}(\psi) = \bar{\mathbf{F}}(\mathbf{p},\dot{\mathbf{p}},\psi) \tag{8}$$

These equations are non-linear parametric ODEs but their dimensions are much reduced compared to the full finite element equations (Eq. (8)). The normal mode mass, stiffness, damping matrix and force vector are given by

$$\begin{aligned} \bar{\mathbf{M}} &= \mathbf{\Phi^T M \Phi} \\ \bar{\mathbf{C}} &= \mathbf{\Phi^T C \Phi} \\ \bar{\mathbf{K}} &= \mathbf{\Phi^T K \Phi} \\ \bar{\mathbf{F}} &= \mathbf{\Phi^T F} \end{aligned} \tag{9}$$

The mode shapes or eigenvectors in Eqs. (9) and (11) are obtained from rotating frequency analysis of the blade which is done by solving an eigenvalue problem given by [19]:

$$\mathbf{K_s \Phi} = \omega^2 \mathbf{M_s \Phi} \tag{10}$$

The blade normal mode equations in Eq. (10) can be written in the following variational form [20]:

$$\int_0^{2\pi} \delta\mathbf{p}^T(\bar{\mathbf{M}}\ddot{\mathbf{p}} + \bar{\mathbf{C}}\dot{\mathbf{p}} + \bar{\mathbf{K}}\mathbf{p} - \bar{\mathbf{F}})d\psi = 0 \tag{11}$$

Integrating Eq. (13) by parts, we obtain [20]

$$\int_0^{2\pi} \begin{Bmatrix} \delta\mathbf{p} \\ \delta\dot{\mathbf{p}}^T \end{Bmatrix} \begin{Bmatrix} \bar{\mathbf{F}} - \bar{\mathbf{C}}\dot{\mathbf{p}} - \bar{\mathbf{K}}\mathbf{p} \\ \bar{\mathbf{M}}\dot{\mathbf{p}} \end{Bmatrix} d\psi = \begin{Bmatrix} \delta\mathbf{p} \\ \delta\dot{\mathbf{p}}^T \end{Bmatrix} \begin{Bmatrix} \mathbf{M}\dot{\mathbf{p}} \\ 0 \end{Bmatrix} \Bigg|_0^{2\pi}$$

Since the helicopter rotor is a periodic system with a time period of one revolution, we have $\dot{\mathbf{p}}(0) = \dot{\mathbf{p}}(2\pi)$. Imposing periodic boundary conditions on Eq. (14) results in the right-hand side becoming zero and yields the following system of first order ordinary differential equations [20] :

$$\int_0^{2\pi} \delta\mathbf{y}^T \mathbf{Q} d\psi = 0$$

where,

$$\mathbf{y} = \begin{Bmatrix} \mathbf{p} \\ \dot{\mathbf{p}} \end{Bmatrix}, \qquad \mathbf{Q} = \begin{Bmatrix} \bar{\mathbf{F}} - \bar{\mathbf{C}}\dot{\mathbf{p}} - \bar{\mathbf{K}}\mathbf{p} \\ \bar{\mathbf{M}}\dot{\mathbf{p}} \end{Bmatrix} \tag{12}$$

The non-linear, periodic, ordinary differential equations are then solved for blade steady response using the finite element in time method [21] and a Newton-Raphson procedure [20]. Discretizing Eq. (15) over N_t time elements around the rotor disk (where $\psi_1 = 0, \psi_{N_t+1} = 2\pi$) and taking a first order Taylor's series expansion about the steady state value $\mathbf{y_0} = [\mathbf{p}_0^T \dot{\mathbf{p}}_0^T]^T$ yields algebraic equations [20]

$$\sum_{i=1}^{N_t} \int_{\psi_i}^{\psi_{i+1}} \delta\mathbf{y}_i^T \mathbf{Q}_i(\mathbf{y}_0 + \Delta\mathbf{y}) d\psi = 0$$

$$\sum_{i=1}^{N_t} \int_{\psi_i}^{\psi_{i+1}} \delta\mathbf{y}_i^T [\mathbf{Q}_i(\mathbf{y}_0) + \mathbf{K}_{ti}(\mathbf{y}_0)\Delta \mathbf{y}] d\psi = 0$$

where,

$$\mathbf{K}_{ti} = \begin{bmatrix} \frac{\partial \bar{\mathbf{F}}}{\partial \mathbf{p}} - \bar{\mathbf{K}} & \frac{\partial \bar{\mathbf{F}}}{\partial \dot{\mathbf{p}}} - \bar{\mathbf{C}} \\ 0 & \bar{\mathbf{M}} \end{bmatrix}_i \tag{13}$$

is the tangential stiffness matrix. For the ith time element, the modal displacement vector can be written as

$$\mathbf{P}_i(\psi) = \mathbf{H}(s)\xi_i \tag{14}$$

where $\mathbf{H}$(s) are time shape functions [21] which are fifth order Lagrange polynomials [20] used for approximating the normal mode co-ordinates $\mathbf{p}$. For a fifth order polynomial, six nodes are needed to describe the variation of $\mathbf{p}$ within the element. Continuity of generalized displacements is assumed between the time elements. Substituting Eq. (17) and its derivative into Eq. (16) yields the time discretized blade response [20]

$$\mathbf{Q}^G + \mathbf{K}_t^G \Delta\xi^G = 0$$

where

$$\mathbf{Q}^G = \sum_{i=1}^{N_t} \int_{\psi_i}^{\psi_{i+1}} \mathbf{H}^T \mathbf{Q}_i d\psi,$$

$$\mathbf{K}_t^G = \sum_{i=1}^{N_t} \int_{\psi_i}^{\psi_{i+1}} \mathbf{H}^T \begin{bmatrix} \frac{\partial \bar{\mathbf{F}}}{\partial \mathbf{p}} - \bar{\mathbf{K}} & \frac{\partial \bar{\mathbf{F}}}{\partial \dot{\mathbf{p}}} - \bar{\mathbf{C}} \\ 0 & \bar{\mathbf{M}} \end{bmatrix}_i d\psi,$$

$$\Delta\xi^G = \sum_{i=1}^{N_t} \Delta\xi_i \tag{15}$$

Solving the above equations iteratively yields the blade steady response.

Steady and vibratory components of the rotating frame blade loads (i.e., shear forces and bending/torsion moments) are calculated using the force summation method [22]. In this approach, blade inertia and aerodynamic forces are integrated directly over the length of the blade. The blade root loads are given as [23]

$$\begin{Bmatrix} F_{xR} \\ F_{yR} \\ F_{zR} \end{Bmatrix} = \int_0^1 \begin{Bmatrix} L_u \\ L_v \\ L_w \end{Bmatrix} dx,$$

$$\begin{Bmatrix} M_{xR} \\ M_{yR} \\ M_{zR} \end{Bmatrix} = \int_0^1 \begin{Bmatrix} -L_v w + L_w v + M_u \\ -L_u w + L_w v + M_v \\ -L_u v + L_v(x+u) + M_w \end{Bmatrix} dx. \tag{16}$$

Fixed frame hub loads are calculated by summing the individual contributions of individual blades [23]:

$$\begin{aligned}
F_x^H(\psi) &= \sum_{m=1}^{N_b} (F_x^m cos\psi_m - F_y^m sin\psi_m \\
&\quad - \beta_p F_z^m cos\psi_m) \\
F_y^H(\psi) &= \sum_{m=1}^{N_b} (F_x^m sin\psi_m - F_y^m cos\psi_m \\
&\quad - \beta_p F_z^m sin\psi_m) \\
F_z^H(\psi) &= \sum_{m=1}^{N_b} (F_z^m + \beta_p F_x^m) \\
M_x^H(\psi) &= \sum_{m=1}^{N_b} (M_x^m cos\psi_m - M_y^m sin\psi_m \\
&\quad - \beta_p M_z^m cos\psi_m) \\
M_y^H(\psi) &= \sum_{m=1}^{N_b} (M_x^m sin\psi_m + M_y^m cos\psi_m \\
&\quad - \beta_p M_z^m sin\psi_m) \\
M_z^H(\psi) &= \sum_{m=1}^{N_b} (M_z^m + \beta_p M_x^m)
\end{aligned}$$

Once the hub loads are obtained, the helicopter needs to be trimmed. Wind tunnel trim procedure is carried out. Wind tunnel trim simulates the test conditions in a wind tunnel. The procedure is to specify the collective pitch, shaft tilt (α_s and ϕ_s) and forward speed and then adjust cyclic pitch (θ_{1c}

and θ_{1s}) to trim the flap angles (β_{1c} and β_{1s}) to zero. As such, the unknown vector to be determined from a modified set of trim equations is,

$$\theta^T = [\theta_{1c}, \theta_{1s}] \tag{17}$$

The fuselage loads and tail rotor are neglected as the HART-II is a main rotor test. Therefore, the longitudinal, lateral and vertical force equilibrium equations need not be satisfied. The expressions for F_4 and F_5 are:

$$F_4 = w_{1c} = \frac{1}{\pi}\int_0^{2\pi} w cos\psi d\psi \tag{18}$$

$$F_5 = w_{1s} = \frac{1}{\pi}\int_0^{2\pi} w sin\psi d\psi \tag{19}$$

In summary, the blade frequencies and mode shapes are obtained and then the blade response around the rotor distrbution is solved for the wind tunnel trim condition. For a real rotor in flight, propulsive trim is used where all three forces and three moments acting on the helicopter are driven to zero.

The UMARC code which contains this analysis was developed at the University of Maryland based on the work of Bir and Chopra and research students [24]. Several versions of the code are now available at different locations. For example, the version at the NASA Ames research center is called the UMARC/A code [25] and the version at Sikorsky aircraft company is called the UMARC/S [26]. In keeping with this nomenclature, we call the version at the Indian Institute of Science as UMARC/I. The results in this paper are therefore for the UMARC/I code.

4 Results and Discussion

4.1 Vibration analysis

The rotor model is developed using data given by HART-II and summarized in Table 1, 2 and 3. Nineteen finite elements are used along the blade span to model the non-uniform rotor blade. The element mesh is shown in Fig. 3. The elements are mostly distributed near the blade inboard region where there is a significant variation in blade structural properties. The outer location of the blade from 44 percent radius to the tip is uniform and needs fewer elements. The frequency diagram and mode shapes of the HART-II blade was computed by a finite element program at German Aerospace Center (DLR). Table 4 shows the comparison of rotating frequencies predicted by UMARC/I and DLR result for the blade for baseline design. A finite element model updating approach is used to tune the baseline model so as to match the test results closely.

Once the basic finite element model is developed and refined for the nominal rotor speed Ω_{ref}, it is used to predict the rotating frequencies for a range of rotor speeds. These results are shown in Fig. 4 as a fan diagram. It can be seen that the fundamental modes show a very good correlation across the spectrum of rotation speeds. The second modes for flap and lag also show quite good correlation. However, for the third flap and first torsion modes, the predicted results are somewhat above the experimental results at lower rotation speeds. Since the helicopter rotor dynamics is adequately captured by the first few modes, it can be concluded that the dynamic model correlates very well with DLR data. In particular, the effect of centrifugal stiffening on the rotating frequency is well captured.

HART-II also provides results for the natural mode shapes. The first three flap modes are shown in Figs. 5, 6 and 7, respectively. The first and second flap modes show good agreement but the third flap mode shows a difference near the root and inboard region. The first and second lag modes are given in Figs. 8 and 9, respectively. The first lag mode correlates very well. However, the phase of the second lag mode is slightly different. The torsion mode is shown in Fig. 10. The torsion mode shape shows some differences near the root region. However, overall it can be said that the mode shapes are quite close to the DLR data. It should also be noted that errors may also be present in the DLR data, especially for higher modes.

Table 4
Rotor blade frequency predictions

Mode	UMARC/I prediction (ω/Ω_{ref})	HART-II Result (ω/Ω_{ref})	Percent Difference
First lag (1L)	0.783	0.782	0.12
First Flap(1F)	1.112	1.125	1.15
Second Lag (2L)	4.584	4.592	0.17
Second Flap (2F)	2.843	2.835	0.28
Third Flap (3F)	5.189	5.168	0.40
First Torsion (1T)	3.844	3.845	0.03

Table 5
Codes used by different teams for HART-II data comparison

TEAM	CODE
Team A	CAMRAD II
Team B	German DLR rotor analysis code, S4
Team C	HOST, METAR, MESIR, MENTHE and ARHIS

Table 6
Higher Harmonic Control input data

Cases	BL(Base line)	MN(Minimum Noise)	MV(Minimum Vibration)
θ_{3c}	–	0.41 deg	−0.79 deg
θ_{3s}	–	−0.70 deg	0.00 deg

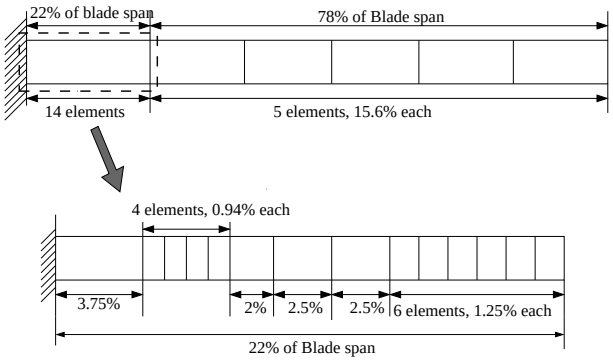

Fig. 3. Finite element mesh used to model the rotor blade

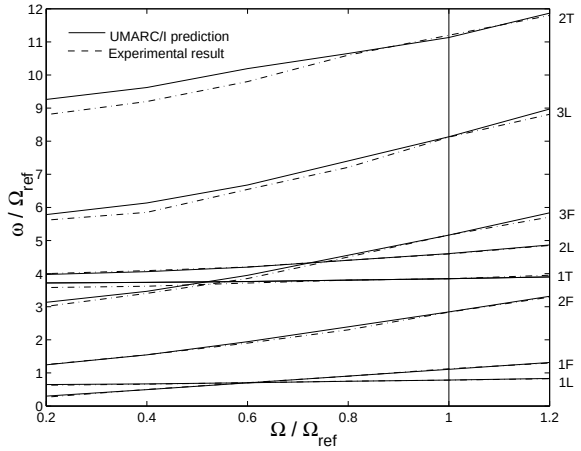

Fig. 4. Comparison of rotor blade frequencies.

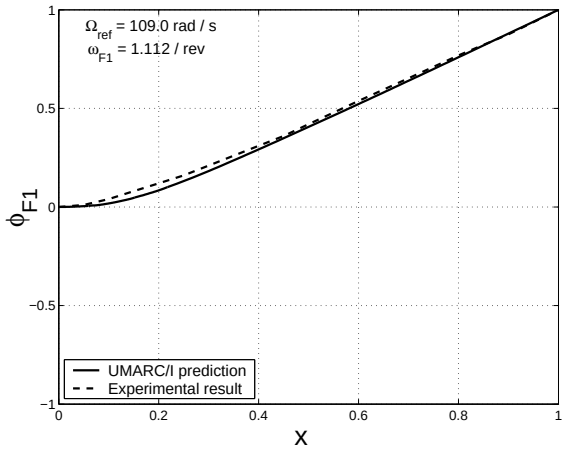

Fig. 5. First flap mode of the rotor blade

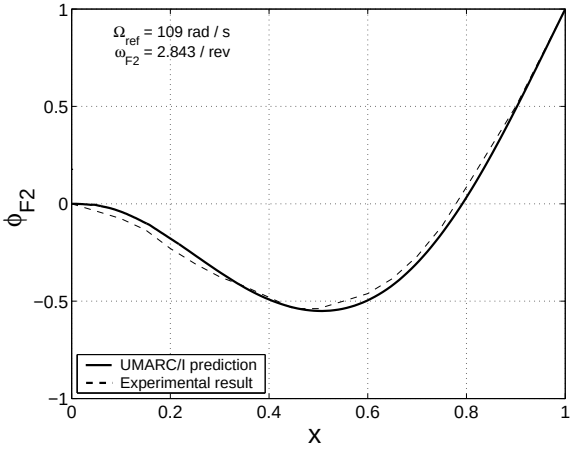

Fig. 6. Second flap mode of the rotor blade

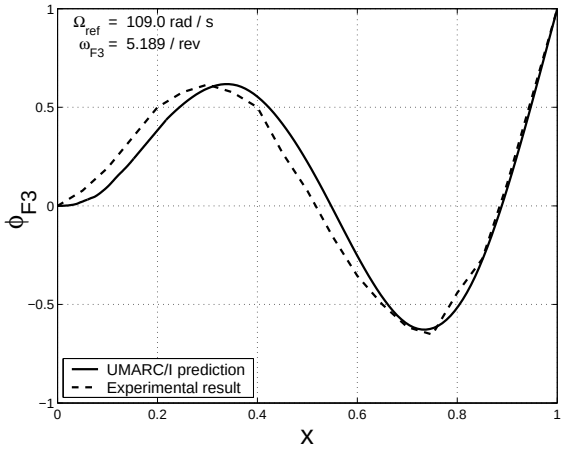

Fig. 7. Third flap mode of the rotor blade

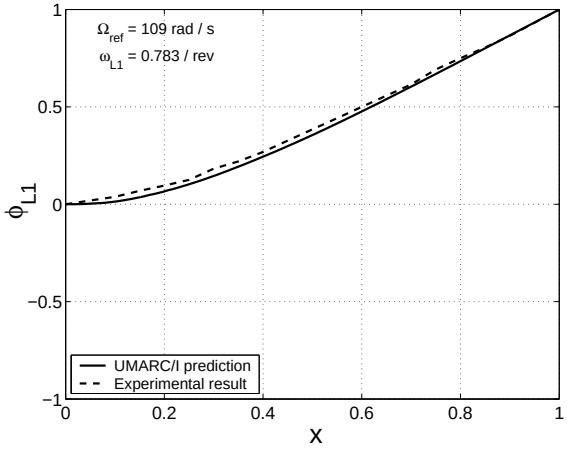

Fig. 8. First lag mode of the rotor blade

4.2 Aeroelastic response

The wind tunnel trim procedure described in section 2 is used to obtain the blade steady state response. This result is then compared

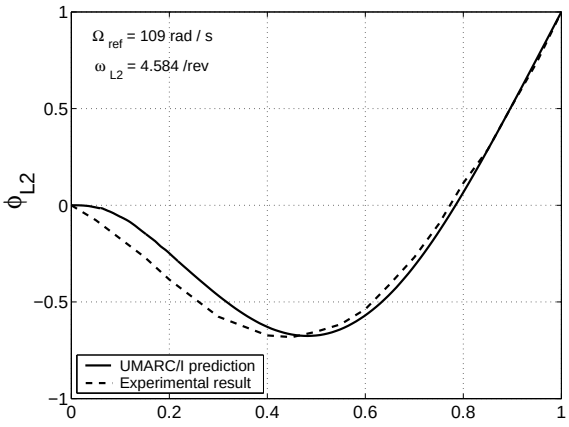

Fig. 9. Second lag mode of the rotor blade

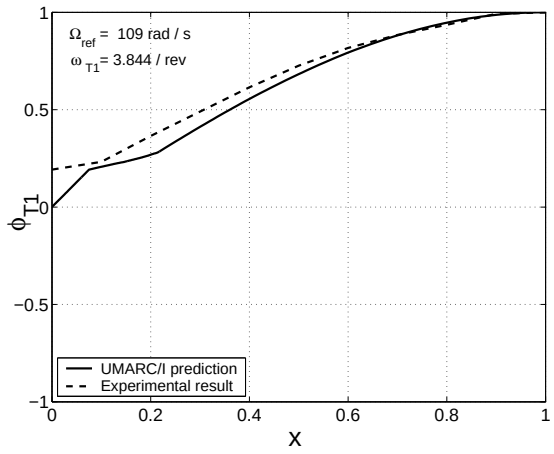

Fig. 10. First torsion mode of the rotor blade

with HART-II experimental data. A low speed flight condition ($\mu = 0.15$) is considered with a shaft forward tilt of 4.5 degrees. It is well known that free wake aerodynamic models are well suited to calculate the effects of rotor wake at low advance ratios [27]. This is because unlike high speed flight, the rotor wake in low speeds remain close to the blade section. Therefore, the free wake model developed by Bagai and Leishman [28] and unsteady aerodynamic model developed by Leishman and Beddoes are used in this study [29,30]. In addition, reverse flow effects are also included.

A comparative study was conducted in Ref [31], where three teams carried out the evaluation using different codes. The description of the teams and their codes are given in Table 5. Figs. 11, 12 and 13 show the time histories of flap, lead-lag and elastic torsion at the blade tip as predicted by UMARC/I and also the results of the three teams in Ref [31]. These results correspond to baseline case. Here the UMARC/I predictions are based on the refined aerodynamic model with free wake and unsteady aerodynamics. The other codes also used their state-of-the art structural and aerodynamic models. The predicted trends of flap response at the blade tip along with the experimental data as well as the prediction of the other three teams is shown in Fig. 11. The predicted flap deflection at the blade tip is in good agreement with the experimental data. Lead-lag response trend is similar to the experimental result but there is a constant offset between the predicted and experimental result for all the codes. However, UMARC/I prediction is much better than the other teams' prediction as shown in Fig. 12. The elastic torsion prediction of UMARC/I and the three teams is as shown in Fig 13. Our prediction is quite good along with Team A and Team C. However, our predictions are not as good around zero degree azimuth and 360 degree azimuth. It should be noted that the accurate prediction of torsion response remains a major issue in helicopter aeroelasticity.

Three flight conditions, Baseline(BL), Minimum Noise(MN) and Minimum vibration(MV) were selected for the study and all these were limited to a shaft tilt of 5.3 degrees. The 3/rev pitch control input was added for minimum noise and minimum vibration cases. Table 6 describes 3 per rev pitch control inputs. The θ_{3c} and θ_{3s} are respectively the cosine and sine components of 3-per-rev higher harmonic pitch input. Figures 14, 15 and 16 show the comparison of flap, lag and torsion response at blade tip for HHC case, respectively. For the flap, all the predicted deflections at the blade tip are in good agreement with the experimental data. The predicted trends in lead-lag tip deflection for MN and MV are similar to the BL case having a constant offset between the experimental data and predicted results. Torsion tip deflection is in good agreement with the experimental data as shown in fig 16.

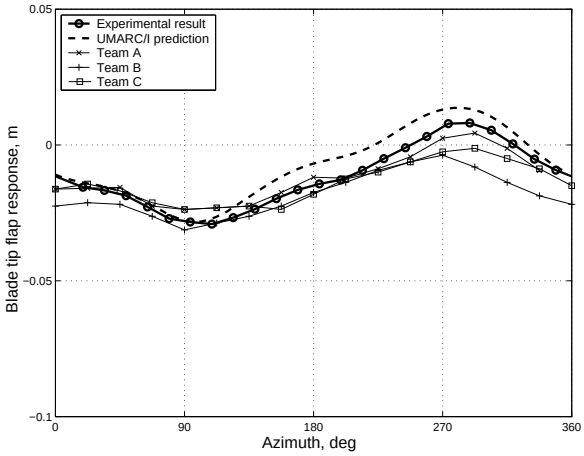

Fig. 11. Comparison of flap response between various codes and experiment(BL)

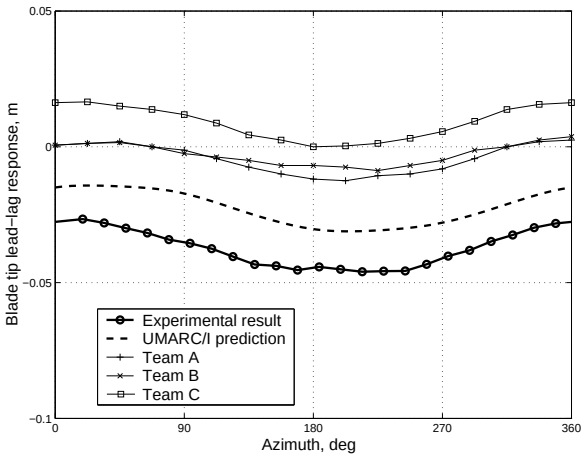

Fig. 12. Comparison of lead-lag response between various codes and experiment(BL)

The flapping of the blade is compared with experimental result in Figs. 17, 18, 19 amd 20 at different azimuths, at 64 deg, 139 deg, 229 deg, 304 deg, respectively. UMARC/I code prediction match with the experimental data except for the MV case at 139 deg, 229 deg and 304 deg. The blade lagging motion is compared in Figs. 21, 22, 23 and 24 at different azimuths 64 deg, 139 deg, 229 deg, 304 deg respectively. The predicted trend of lead-lag results are similar to the experimental data but there are constant offset between the predicted result and the experimental result at all the azimuths. A comparison of torsion results is done in Figs. 25, 26, 27 and 28 at 64 deg, 139 deg, 229 deg, 304 deg azimuth respectively. At 64 deg azimuth (Fig. 25), MN is captured better than BL and MV. At 139 deg azimuth (Fig. 26), trend of MN case is not matching the experimental result. At 229 deg azimuth(Fig. 27), in all the three cases, we were underpredicting the experimental result. At 304 deg azimuth (Fig. 28), MN case is in good agreement with the experimental data.

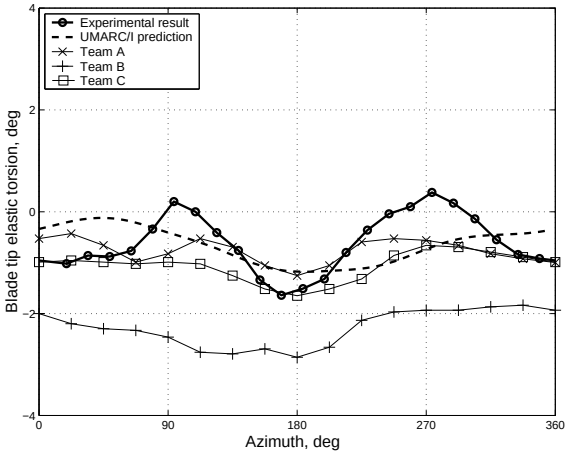

Fig. 13. Comparison of torsion response between various codes and experiment(BL)

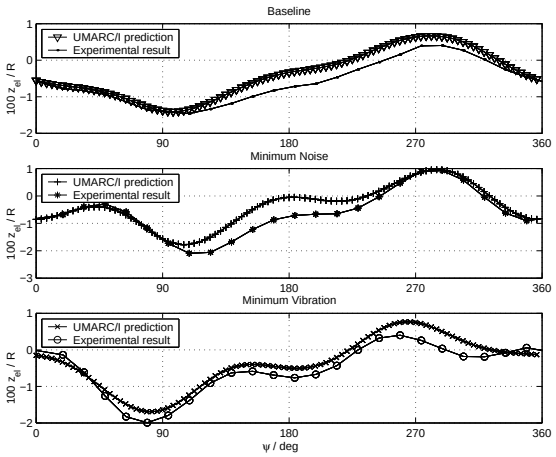

Fig. 14. Comparison of flap response for HHC cases

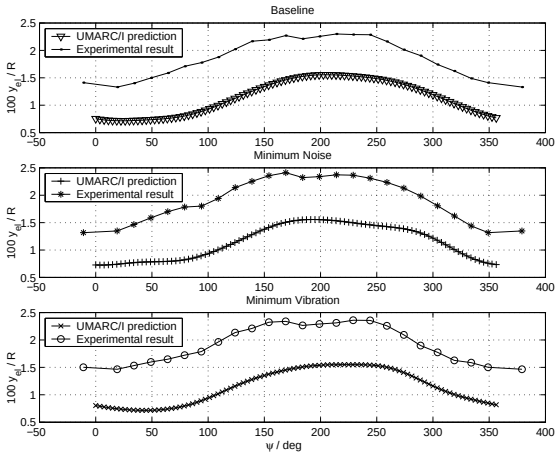

Fig. 15. Comparison of lag response for HHC cases

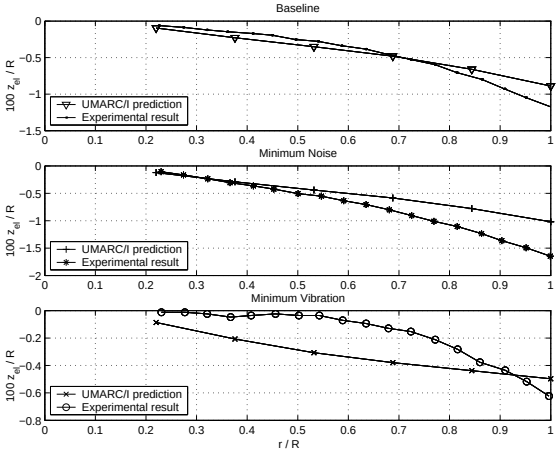

Fig. 18. Comparison of elastic flapping of blade, $\psi = 139\,\mathrm{deg}$

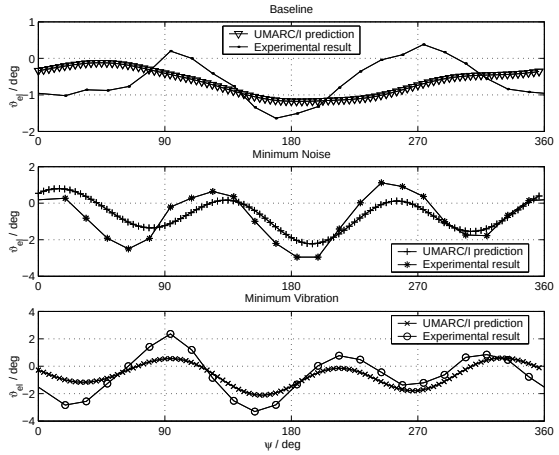

Fig. 16. Comparison of torsion response for HHC cases

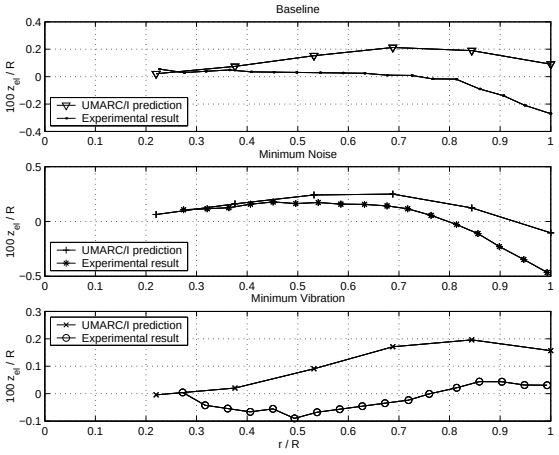

Fig. 19. Comparison of elastic flapping of blade, $\psi = 229\,\mathrm{deg}$

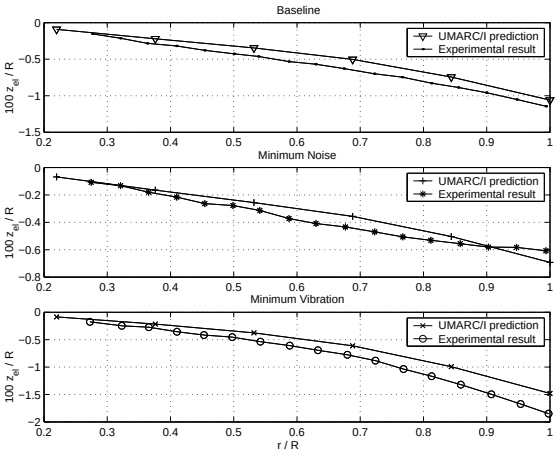

Fig. 17. Comparison of elastic flapping of blade, $\psi = 64\,\mathrm{deg}$

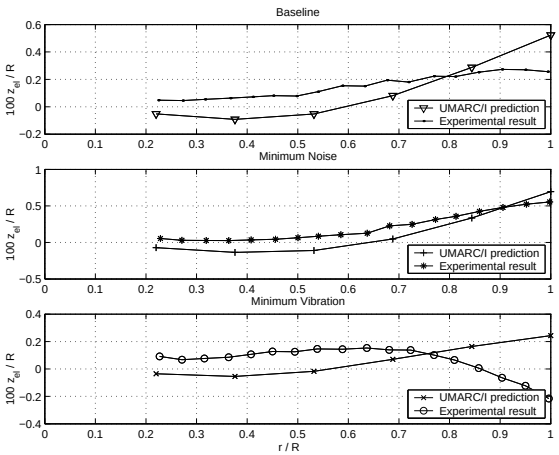

Fig. 20. Comparison of elastic flapping of blade, $\psi = 304\,\mathrm{deg}$

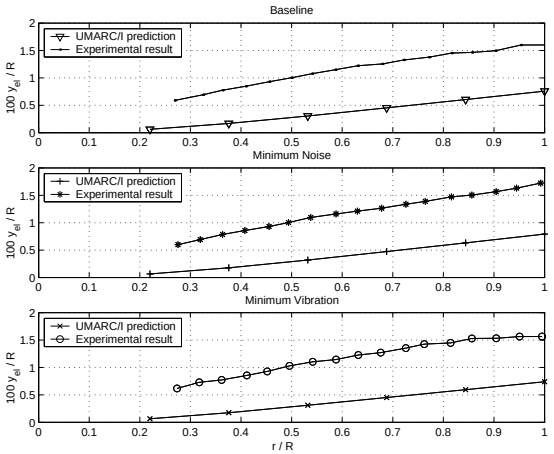

Fig. 21. Comparison of elastic lagging of blade, $\psi = 64\,\mathrm{deg}$

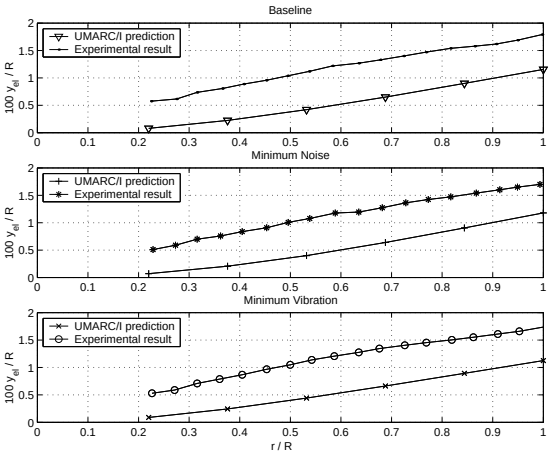

Fig. 24. Comparison of elastic lagging of blade, $\psi = 304\,\mathrm{deg}$

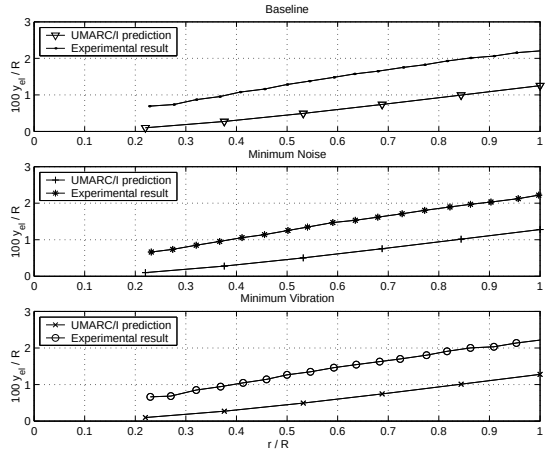

Fig. 22. Comparison of elastic lagging of blade, $\psi = 139\,\mathrm{deg}$

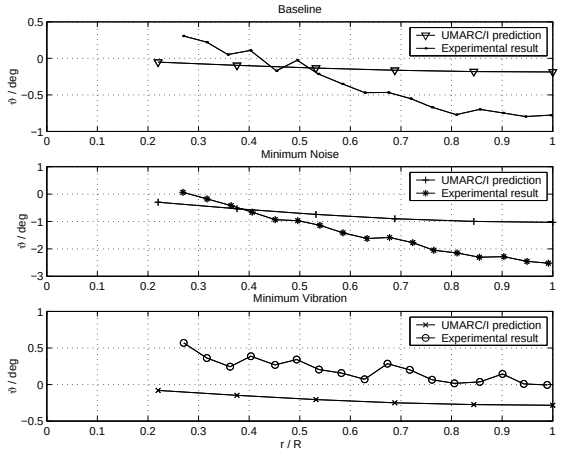

Fig. 25. Comparison of elastic torsion of blade, $\psi = 64\,\mathrm{deg}$

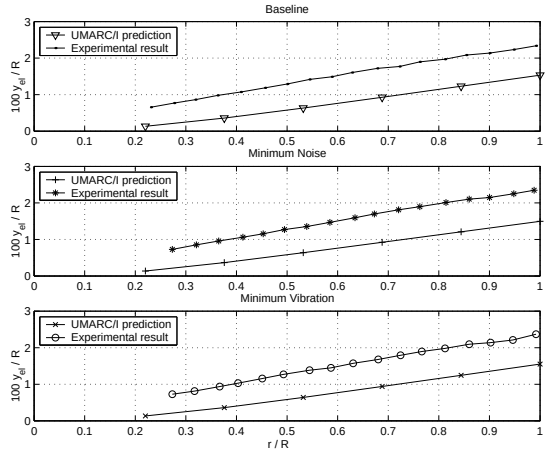

Fig. 23. Comparison of elastic lagging of blade, $\psi = 229\,\mathrm{deg}$

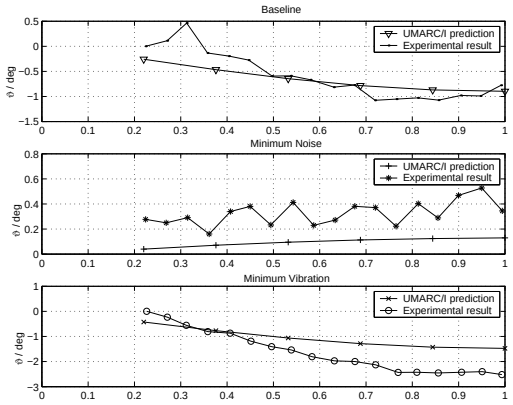

Fig. 26. Comparison of elastic torsion of blade, $\psi = 139\,\mathrm{deg}$

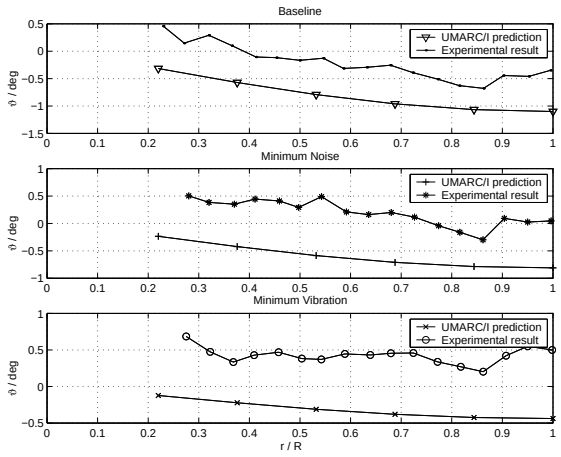

Fig. 27. Comparison of elastic torsion of blade, $\psi = 229\,\mathrm{deg}$

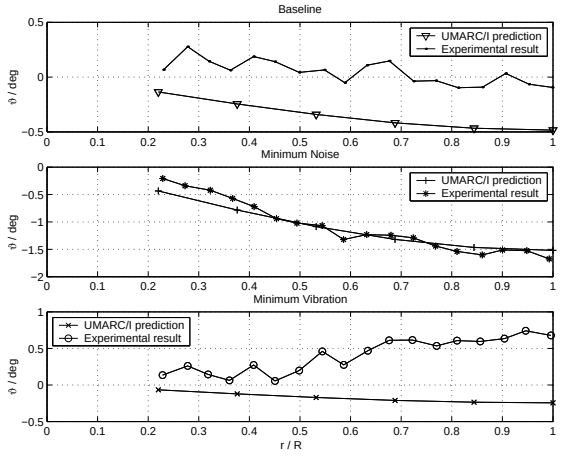

Fig. 28. Comparison of elastic torsion of blade, $\psi = 304\,\mathrm{deg}$

5 Conclusion

Numerical results from a comprehensive aeroelastic analysis are compared with wind tunnel data obtained in the HART-II tests. Good correlation is obtained for the rotating frequencies across a range of rotating speeds. The basic physics of the mode shapes is also well captured. In particular, the fundamental flap, lag and torsion modes compare very well. The periodic response around the rotor distribution compares well with the experimental result and other code predictions for flap mode. For the lag mode, our prediction is somewhat better than the other codes. The torsion response prediction is also reasonably good. While the basic physics appears to be well captured by the aeroelastic analysis, there is need for improvement in the aerodynamic modeling which appears to be the source of the gap between predictions and experiments. The predicted results of blade deflections for the HHC case were fair when compared with the experimental data, but there were constant offsets in the mean values for lead-lag and elastic torsion.
An effort to understand the source of these prediction shortcoming is a subject of future work. It is likely that accurate aerodynamic modeling such as the use of CFD is needed to improve the predictive capacity of the aeroelastic code.

6 Acknowledgement

The authors are grateful to Dr. Berend van der Wall for providing the HART-II data and to Dr. Joon W. Lim for his comments on the paper.

Nomenclature

C_t thrust coefficient
EI_y flap bending stiffness
EI_z lag bending stiffness
e_g location of centre of gravity from elastic axis (+ve toward leading edge).
e_A location of tension center from elastic axis (+ve toward leading edge).
e_d location of aerodynamic center from elastic axis (+ve toward trailing edge).
F hub forces
F_x longitudinal hub forces
F_y lateral hub forces
F_z vertical hub forces
$\mathbf{F}$ finite element force vector
F_4 rolling moment equilibrium residual about the vehicle cg
F_5 pitching moment equilibrium residual about the vehicle cg
GJ torsional stiffness
H time shape function
J objective function
K finite element stiffness matrix
$\mathbf{K_s}$ finite element structural stiffness matrix
$L_u$blade section lift in axial direction
$L_v$blade section lift in lag direction
$L_w$blade section lift in flap direction
L_u^A, L_u^A, L_u^A distributed air loads in x, y and z directions respectively
M_u blade section moment in axial direction
M_v blade section moment in lag direction
$M_w$blade section moment in flap direction
$M_x$rolling moment
$M_y$pitching moment
$M_z$yawing moment
M hub moments
$M_{\hat{\phi}}^A$ aerodynamic pitching moment about undeformed elastic axis
$\mathbf{M}$ finite element mass matrix
$\mathbf{M_s}$ finite element structural mass matrix
N number of spatial finite elements
N_t number of time finite elements
$\mathbf{p}$ normal mode co-ordinate vector
$\mathbf{q}$ finite element nodal displacement vector
s local time co-ordinate
u axial deflection of the blade
v lag bending deflection of the blade
w flap bending deflection of the blade
x spatial coordinate along the blade
δ variation
θ helicopter trim control angles
θ_{1c}, θ_{1s} lateral and longitudinal cyclic trim inputs, respectively
ψ rotor azimuth angle
$\hat{\phi}$ torsion response
Φ mode shape
μ advance ratio
ω rotating frequency
Ω rotor rotational speed

References

[1] Lim, J.W., Tung, C. and Yu, Y.H. Prediction of blade-vortex interaction airloads with higher harmonic pitch controls using the 2GCHAS Comprehensive Code, *Journal of Pressure Vessel Technology*, 2001, **123**,(4), pp 469-474.

[2] Lim, J.W. and Anastassiades, T. Correlation of 2GCHAS analysis with experimental data, *Journal of the American Helicopter Society*, 1995, **40**,(4), pp 18-33.

[3] Yeo, H., Bousman, W.G. and Johnson,W. Performance analysis of a utility helicopter with standard and advanced rotors, *Journal of the American Helicopter Society*, 2004, **49**,(3), pp 250-270.

[4] Lim, J.W., Yu, Y.H. and Johnson, H. Calculation of the rotor blade-vortex interaction airloads using a multiple trailer free-wake model, *Journal of Aircraft*, 2003,**40**,(6), pp1123-1130.

[5] Hansford, R.E. and Vorwald, J. Dynamics workshop on rotor vibrating loads prediction, *Journal of the American Helicopter Society*, 1998, **43**,(1), pp 76-87.

[6] Ganguli, R., Chopra, I. and Weller, W.H. Comparison of Calculated Vibratory Rotor Hub Loads with Experimental Data, *Journal of the American Helicopter Society*, 1998, **43**,(4), pp 312-318.

[7] Davis, M.W. and Weller, W.H. Helicopter Rotor Dynamics Optimization with Experimental Verification, *Journal of Aircraft*, 1991, **28**,(1), pp 38-48.

[8] Davis, M.W. and Weller, W.H. A Modal based Procedure for Efficiently Predicting Low Vibration Rotor Designs, *Journal of the American Helicopter Society*, 1993, **38**,(1), pp 62-72.

[9] Datta, A. and Chopra, I. Validation of Structural and Aerodynamic modeling using UH-60A Flight Test Data, *59th Annual Forum of the American Helicopter Society* , Arizona, May2003.

[10] Nguyen, K., Betzina, M. and Kitaplioglu, C. Full-Scale Demonstration of Higher Harmonic Control for Noise and Vibration Reduction on the XV-15 Rotor, *Journal of The American Helicopter Society*, 2001, **46**,(3), pp 182-191.

[11] Nixon, M., Kvaternik, R. and Settle, T. Tiltrotor Vibration Reduction Through Higher Harmonic Control, *Journal of The American Helicopter Society*, 1998, bf34,(3), pp 235-256.

[12] Van der Wall, B.G. 2^{nd} HHC Aeroacoustic Rotor Test (HART-II)- Part I: Test Documentation, DLR IB-111 – 2003/31, Braunschweig, Germany, Nov 2003.

[13] Van der Wall, B.G. 2^{nd} HHC Aeroacoustic Rotor Test (HART-II)- Part II: Representative Results, DLR IB-111 – 2005/03, Braunschweig, Germany, Feb 2005.

[14] Yu, Y.H., Tung, C., Van der Wall, B.G., Pausder, H.J., Burley, C.L., Brooks, T.F., Beaumier, P., Delrieux, Y. Mercker, E., Pengel, K. The HART-II Test: Rotor Wakes and Aeroacoustics with Higher Harmonic Pitch Control (HHC) inputs-The Joint German/French/Dutch/US project, *58th Annual Forum of the American Helicopter Society*, Montreal, Canada, 2002.

[15] Van der Wall, B.G., Schneider, O., Pengel, K. HART-II Blade Motion Measured by Stereo Pattern Recognition(SPR), *59th Annual Forum of the American Helicopter Society* , Arizona, 2003.

[16] Van der Wall, B.G., Junker, B., Burley, C.L., Brooks, T.F., Yu, Y.H., Tung, C. Beaumier, P., Delrieux, Y., Mercker, E., Pengel, K., Holthusen, H., Raffel, M., Richard, H., Wagner, W. The HART-II

Test in the LLF of the DNW- a major step towards Rotor Wake Understanding, *28th European Rotorcraft Forum*, Bristol, England, 2002.

[17] Pengel, K., Mueller, H.G., Van der Wall, B.G. Stero Pattern Recognition-the technique for reliable rotor blade deformation and twist measurement, Heli Japan, *AHS International meeting on advanced rotorcraft technology and life saving activities*, Tochigi, Japan, 2002.

[18] Van der Wall, B.G., Burley, C.L., Yu, Y.H., Richard, H., Pengel, K., Beaumier, P. The HART-II test-measurement of helicopter rotor wakes, *Aerospace Science and Technology*, Jun 2004, **8**,(4), pp 273-284.

[19] Chopra, I., Sivaneri, N.T. Aeroelastic stability of rotor blades using finite element analysis. NASA CR 166389. 1982.

[20] Lim, J.W. and Chopra, I. Aeroelastic optimization of a helicopter using an efficient sensitivity analysis, *Journal of Aircraft*, 1991. **28**,(1), pp 29-37

[21] Borri, M. Helicopter rotor dynamics by finite element time approximation, *Computer and Mathematics with Appications*, 1986, **12A**,(1), pp 149-160.

[22] Hansford, R.E A uniform formulation of rotor loads prediction methods, *Journal of the American Helicopter Society*, 1986, 31, pp 58-65.

[23] Ganguli, R. Aeroelastic optimization of advanced geometry and composite helicopter rotors, Ph.D Dissertation, University of Maryland at College Park, MD, U.S.A, 1994.

[24] Bir, G.S., Chopra, I., Ganguli, R. et. al., University of Maryland Advanced Rotorcraft Code (UMARC). Theory manual, Center for Rotorcraft Education and Research, University of Maryland, College Park, July 1994.

[25] Nugyen, K. Active control of helicopter blade stall, *Journal of Aircraft*, 1998, **35**,(1), pp 91-98.

[26] Torok, M.S. Aeroelastic analysis of active rotor control concepts for vibratory reduction, *American Helicopter Society Annual Forum*, 1996, 1, pp 111-122.

[27] Conlisk, A.T. Modern Helicopter rotor aerodynamics, Progress in Aerospace Sciences, 2001, **37**,(5), pp 419-476.

[28] Bagai, A., Leishman, J.G. Rotor Free Wake modeling using a Pseudo-Implicit Technique- Including Comparisons with Experiment, *Journal of the American Helicopter Society*, July 1995, **40**,(3), pp 29-41

[29] Leishman, G.J. Validation of Approximate Indicial Aerodynamic Functions for Two-dimensional Subsonic Flow, *Journal of Aircraft*, Oct 1998, **25**,(1), pp 914-922.

[30] Beddoes, T.S. Practical Computation of Unsteady Lift, *Proceedings of the 7th European Rotorcraft Forum*, Sep 1982, see also *Vertica*, 1984, **8**,(1), pp 55-71.

[31] Lim, J.W., Burley, C.L., Byod, D., Van der Wall, B.G., Schneider, O., Brooks, T.F., Yu, Y.H., Tung, C., Beaumier, P., Bailly, J., Delrieux, Y., Mercker, E., Pengel, K., Raffel, M., Richard, H. HART-II: Prediction of Blade Vortex Interaction Loading, *29th European Rotorcraft Forum*, Friedrichshafen, Germany, Sep 2003.

Appendix

$$\frac{\delta U}{m_0\Omega^2R^3} = \int_0^1 (U_{u'_e}\delta u'_e$$

$$+\mathrm{U}_{v'}\delta v' + U_{w'}\delta w' + U_{v''}\delta v''$$

$$+ \mathrm{U}_{w''}\delta w'' + U_{\hat{\phi}}\delta\hat{\phi}$$

$$+\mathrm{U}_{\hat{\phi}'}\delta\hat{\phi}' + U_{\hat{\phi}''}\delta\hat{\phi}'')dx$$

where,

$$\mathrm{U}_{u'_e} = EA\left[u'_e + k_A^2\theta'_0(\hat{\phi}' + w'v'') + k_A^2\frac{\hat{\phi}'^2}{2}\right]$$

$$-\ \mathrm{EAe}_A\left[v''(cos\theta_0 - \hat{\phi}sin\theta_0) + w''(sin\theta_0 + \hat{\phi}cos\theta_0)\right]\beta_p + 2\dot{v'}e_gcos\theta_0 + 2\dot{w'}e_gsin\theta_0 - \ddot{v} + \hat{\phi}e_gsin\theta_0$$

$$\mathrm{U}_{v''} = v''(EI_zcos^2\theta_0 + EI_ysin^2\theta_0)$$

$$+\ \mathrm{w}''(EI_z - EI_y)cos\theta_0sin\theta_0$$

$$-\ \mathrm{EAe}_Au'_e(cos\theta_0 - \hat{\phi}sin\theta_0) - \hat{\phi}'EB_2\theta'_0cos\theta_0$$

$$+\ \mathrm{w}''\hat{\phi}(EI_z - EI_y)cos2\theta_0 - v''\hat{\phi}(EI_z - EI_y)sin2\theta_0$$

$$+\ (\mathrm{GJ} + \mathrm{EB}_1\theta_0'^2)\hat{\phi}'w' + EAk_A^2\theta'_0w'u'_e$$

$$\mathrm{U}_{w'} = (GJ + EB_1\theta_0'^2)\hat{\phi}'v'' + EAk_A^2\theta'_0v''u'_e$$

$$\mathrm{U}_{w''} = w''(EI_ycos^2\theta_0 + EI_zsin^2\theta_0) + v''(EI_z - EI_y)cos\theta_0sin\theta_0$$

$$-\ \mathrm{EAe}_Au'_e(sin\theta_0 + \hat{\phi}cos\theta_0) - \hat{\phi}'EB_2\theta'_0sin\theta_0$$

$$+\ \mathrm{w}''\phi(EI_z - EI_y)sin2\theta_0 + v''\hat{\phi}(EI_z - EI_y)cos2\theta_0$$

$$\mathrm{U}_{\hat{\phi}} = w''^2(EI_z - EI_y)cos\theta_0sin\theta_0 + v''w''(EI_z - EI_y)cos2\theta_0$$

$$-\ \mathrm{v}''^2(EI_z - EI_y)cos\theta_0sin\theta_0$$

$$\mathrm{U}_{\hat{\phi}'} = GJ(\hat{\phi}' + w'v'') + EB_1\theta_0'^2\hat{\phi}' + EAk_A^2(\theta'_0 + \hat{\phi}')u'_e$$

$$-\ \mathrm{EB}_2\theta'(v''cos\theta_0 + w''sin\theta_0)$$

$$\mathrm{U}_{\hat{\phi}''} = EC_1\hat{\phi}'' + EC_2(w''cos\theta_0 - v''sin\theta_0)$$

$$\frac{\delta T}{m_0\Omega^2R^3} = \int_0^1 m(T_{u_e}\delta u_e + T_v\delta v + T_w\delta w + T_{v'}\delta v' + T_{w'}\delta w' + T_\phi\delta\phi + T_F)dx$$

where,

$$\mathrm{T}_{u_e} = x + u_e + 2\dot{v} - \ddot{u}_e$$

$$\mathrm{T}_v = e_g(cos\theta_0 + \ddot{\theta}_0sin\theta_0) + v - \hat{\phi}e_gsin\theta_0 +$$

$$-\ 2 + 2\int_0^x(v'\dot{v'} + w'\dot{w'})d\xi$$

$$\mathrm{T}_{v'} = -e_g(xcos\theta_0 - \hat{\phi}xsin\theta_0 + 2\dot{v}cos\theta_0)$$

$$\mathrm{T}_w = -x\beta_p - \ddot{\theta}_0e_gcos\theta_0 - 2\dot{v}\beta_p - \ddot{w} - \ddot{\hat{\phi}}e_gcos\theta_0$$

$$\mathrm{T}_{w'} = -e_g(xsin\theta_0 + \hat{\phi}xcos\theta_0 + 2\dot{v}sin\theta_0)$$

$$\mathrm{T}_{\hat{\phi}} = -k_m{}^2\ddot{\hat{\phi}} - (k_{m2}{}^2 - k_{m1}{}^2)cos\theta_0sin\theta_0 - x\beta_pe_gcos\theta_0$$

$$-\ \mathrm{v}\ e_gsin\theta_0 + v'xe_gsin\theta_0 - w'xe_gcos\theta_0 + \ddot{v}e_gsin\theta_0$$

$$-\ (\mathrm{k}_{m2}^2 - k_{m1}{}^2)cos2\theta_0 - \ddot{w}e_gcos\theta_0 - k_m^2\ddot{\theta}_0$$

$$\mathrm{T}_F = -(x + 2\dot{v})\int_0^x(v'\delta v' + w'\delta w')d\xi$$

$$\delta W = \int_0^R(L_u^A\delta u + L_v^A\delta v + L_w^A\delta w + M_{\hat{\phi}}^A\delta\hat{\phi})$$